Crystal Structure of Archaeal Ribonuclease P Protein aRpp29 from *Archaeoglobus fulgidus*[†,‡]

David J. Sidote, Johanna Heideker, and David W. Hoffman*

Department of Chemistry and Biochemistry, Institute for Cellular and Molecular Biology, University of Texas, Austin, Texas 78712

Received July 5, 2004; Revised Manuscript Received August 26, 2004

ABSTRACT: The crystal structure of ribonuclease P protein aRpp29 from the sulfate-reducing hyperthermophile *Archaeoglobus fulgidus* was determined at 1.7 Å resolution using X-ray diffraction methods. The central feature of this archaeal protein is a sheet of six antiparallel β-strands twisted around a conserved hydrophobic core. Residues near the N- and C-termini form helical structures that are oriented in an antiparallel manner. A comparison of conserved amino acids indicates that archaeal aRpp29 is homologous to human ribonuclease P protein Rpp29. The aRpp29 protein is structurally similar to bacterial transcription factors Hfq and NusG, as well as the Sm and Sm-like RNA-associated proteins from eukarya. The crystal structure of *A. fulgidus* aRpp29 differs from the previously reported solution structure, where NMR data did not detect the helices and indicated that ∼40% of the residues are relatively flexible or disordered. Circular dichroism data indicate that the protein has less helical content than the amount observed in the crystal, suggesting that in solution the helical regions are unfolded or in equilibrium between folded and unfolded forms; this hypothesis is consistent with amide proton exchange rate data. Surface residues that are conserved from archaea to humans and are likely to interact with the ribonuclease P RNA or other protein subunits are identified in the structure. The model of the aRpp29 protein defined by this work provides an essential step toward eventually understanding the overall architecture of ribonuclease P.

The precursors of transfer RNAs (pre-tRNAs) require extensive modification prior to maturation. These post-transcriptional alterations consist of the removal of the 5′ leader sequence, intron splicing in archaea and eukarya, addition of the 3′ CCA nucleotides, and base modifications. Ribonuclease P (RNase P) is the ribonucleoprotein enzyme responsible for removal of the leader sequence at the 5′ end of pre-tRNA (*1*). RNase P is present in bacteria, archaea, eukarya, and organelles that perform translation (*2*, *3*). Bacterial RNase P is a relatively simple form of the enzyme and the best characterized example. It consists of an RNA component 350−400 nucleotides in length and a single 14 kDa protein subunit (*4*). The bacterial RNA alone can catalyze the cleavage of pre-tRNA in the absence of the protein subunit under conditions of high ionic strength, although the protein is necessary for the enzyme to function efficiently under physiological conditions (*4*−*6*); the protein subunit also facilitates substrate recognition and release (*7*). In contrast to the bacterial enzyme, eukaryotic RNase P is significantly larger and more complex. The human and yeast forms of RNase P each contain a single RNA subunit approximately 400 nucleotides in length, and at least nine protein subunits ranging in size from 14 to 100 kDa (*8*, *9*). The archaeal RNase P contains a single RNA subunit with a length of 227−400 nucleotides, depending on species, and at least four protein subunits ranging in size from 11 to 23 kDa (*10*). Archaeal RNase P therefore appears to be intermediate in complexity between that of bacteria and eukarya.

Comparisons of amino acid sequences indicate that the four known archaeal RNase P proteins are similar to human proteins Rpp29 (Pop4 in yeast), hPop5 (Pop5 in yeast), Rpp21 (Rpr2 in yeast), and Rpp30 (Rpp1 in yeast) (*10*, *11*). No such homology appears to exist between the bacterial RNase P protein and the RNase P proteins of archaea or eukarya. Phylogenetic analyses have been used to classify archaeal RNase P as either type A, which has an RNA core component that is similar to that found in bacteria, or type M, which appears to be missing two substrate recognition elements (*12*). In the absence of the protein subunits, the type A RNase P RNA from some species of archaea has been induced to cleave pre-tRNA under extreme ionic conditions (*6*).

Since the discovery of RNase P as one of the first examples of a ribozyme (*5*), there continues to be a very strong interest in this ancient and well-conserved ribonucleoprotien particle (reviewed in refs *13* and *14*). Significantly, however, RNase P differs from a number of other well-known ribozymes in that there is a relative lack of detailed structural information available for the full particle, as well as many of the components. For example, in the past several years, detailed three-dimensional structures have been reported for the hammerhead ribozyme (*15*, *16*), hepatitus delta virus ribozyme (*17*, *18*), group I ribozyme domain (*19*),

[†] This work was supported by Grant F-1353 from the Welch Foundation.

[‡] Protein Data Bank entries 1TS9 and 1TSF.

* To whom correspondence should be addressed: Department of Chemistry and Biochemistry, Institute for Cellular and Molecular Biology, University of Texas, Austin, TX 78712. E-mail: dhoffman@mail.utexas.edu. Phone: (512) 471-7859. Fax: (512) 471-8696.

10.1021/bi048578z CCC: $27.50
Published on Web 10/16/2004

leadzyme (*20*), and the ribosome (*21*, *22*), while our understanding of the RNase P structure remains relatively sparse. A thorough understanding of the mechanism and function of RNase P will certainly require that detailed structural information be available, like that which can be provided by X-ray crystallography or NMR methods.

Bacterial RNase P is significantly better characterized than the eukaryotic or archaeal forms of the enzyme. Although the structure of the complete bacterial RNase P has not yet been determined, there is substantial information regarding the structures of some of the individual components and the overall architecture. The structure of the 154-nucleotide specificity domain of the *Bacillus subtilis* RNase P RNA was recently determined using crystallographic methods (*23*), and three-dimensional models of the *Escherichia coli* and *B. subtilis* RNA have been constructed using comparative phylogenetic analysis (*24*). The structure of the bacterial protein subunit from *B. subtilis* has been determined using NMR[1] (*25*), and the structures of the protein subunit from *Streptomyces aureus* and *Thermotoga maritima* have been determined by X-ray crystallography (*26*, *27*). Although no structures of any of the eukaryotic RNase P components have been directly determined, the structures of archaeal RNase P proteins that are homologues of two human and yeast proteins are now known. The solution structures of the *Archaeoglobus fulgidus* and *Methanothermobacter thermoautotrophicus* proteins that are similar to human RNase P protein Rpp29 were recently determined using NMR methods (*28*, *29*), and the crystal structures of the *Pyrococcus horikoshii* proteins that are the similar to human Rpp30 and Rpp29 were recently determined by X-ray diffraction (*30*, *31*).

The *A. fulgidus* RNase P protein aRpp29[1] (similar to the human protein Rpp29 and the yeast protein Pop4) is the subject of the structural and biophysical studies described here. This protein is significant for several reasons. Interaction maps derived from two- and three-hybrid assays indicate that the yeast and human homologues of aRpp29 directly contact the RNA component of RNase P, and are involved in a relatively large number of protein−protein interactions (*9*, *32*), although the specific sites of interaction are unknown. aRpp29 is the only RNase P protein with homologues identified in all eukarya and archaea with available genome sequences (*13*), and it has recently been reported that a eukaryotic Rpp29 protein and the *E. coli* RNase P RNA by themselves form a complex with catalytic activity (*33*). Taken together, these observations provide evidence for the importance of aRpp29 and its homologues in RNase P structure and function.

A. fulgidus is a hyperthermophilic sulfate-reducing organism with an optimal growth temperature of 83 °C. The *A. fulgidus* RNase P has several characteristics that make it an excellent candidate for structural studies. It has a relatively small, type M, RNA component containing only 229 nucleotides. The *A. fulgidus* genome has been sequenced, facilitating the identification of components that interact with RNase P. In addition, *A. fulgidus* can be cultured in the laboratory, which may prove important in future studies of RNase P.

[1] Abbreviations: aRpp29, archaeal RNase P protein 29; NMR, nuclear magnetic resonance; NOE, nuclear Overhauser effect; SeMet, selenomethionine.

Previous NMR studies of *A. fulgidus* aRpp29 show that the central structural feature of this 102-residue protein is a sheet of six antiparallel β-strands, wrapped around a core of conserved hydrophobic amino acids (*28*). In contrast to the relatively rigid and well-defined β-sheet, approximately 40% of the protein was poorly defined in solution; this includes the first 16 residues, located before the start of the first β-strand, and the last 24 residues, located past the end of the last β-strand. The apparent flexibility of the N- and C-terminal regions of aRpp29 might have indicated that it is a poor candidate for crystallization; however, the protein was found to crystallize quite well, and diffract X-rays to high resolution. Here we describe the crystal structure of *A. fulgidus* aRpp29 and, in addition, reconcile and interpret the differences between the crystal and solution structures of the protein.

EXPERIMENTAL PROCEDURES

Crystallization and X-ray Diffraction. The 102-amino acid archaeal homologue of the human RNase P protein Rpp29 (aRpp29) was cloned from *A. fulgidus* genomic DNA and expressed as a fusion with maltose binding protein. Following cleavage of the fusion with tobacco etch virus (TEV) protease, the protein was purified to homogeneity as previously described (*28*). The protein was crystallized using the hanging drop vapor diffusion method with samples at concentrations of 15 mg/mL. Native crystals were grown in 0.1 M sodium citrate (pH 5.5) and 2.2 M ammonium sulfate at room temperature, with crystal formation occurring after 2 months. Protein-containing selenomethionine was produced as described by VanDuyne *et al.* (*34*), and purified exactly as the native protein. Crystals of the selenomethionine form of aRpp29 were grown from a solution of 0.1 M HEPES (pH 7.5) and 1.2 M ammonium sulfate, with crystal formation occurring after 4−5 days at room temperature. Crystals were transferred to a 25% glycerol cryoprotectant solution for 1 min prior to freezing, removed from the cryoprotectant using a nylon loop (Hampton Research), and frozen in the nitrogen stream at 100 K. X-ray diffraction data at 1.54 Å were collected for the native and selenomethionine forms using a rotating copper anode X-ray source equipped with a MAR3450 detector (MAR-USA, Inc.). Synchrotron data were collected for the selenomethionine form at the PX beamline at the Center for Advanced Microstructures and Devices (CAMD) in Baton Rouge, LA, equipped with a MAR CCD detector (MAR-USA, Inc.); data were collected at 0.97945 Å, corresponding to the peak selenium anomalous signal according to a fluorescence scan. Diffraction data were integrated and scaled using DENZO and SCALEPACK (*35*) to a resolution of 1.7 Å.

Crystal Structure Determination and Refinement. The crystal structure of the selenomethionine form of aRpp29 was determined using the single-wavelength anomalous dispersion (SAD) method. The locations of the five selenium atoms and initial phases were calculated at 3.5 Å using SHARP (*36*). After solvent flattening was carried out using ARP/warp (*37*), a model of the structure was built into the electron density using XtalView (*38*). After positional refinement, density modification was repeated at 1.8 Å to improve the phases, followed by multiple cycles of rebuilding (using omit maps) and positional refinement using the

Table 1: Structure Determination and Refinement Statistics[a]

	native (Cu K)	SeMet (Cu K)	SeMet (CAMD)
space group	$P2_12_12_1$	$P2_12_12$	$P2_12_12$
cell constants	$a = 39.6$ Å $b = 43.8$ Å $c = 49.2$ Å $\alpha, \beta, \gamma = 90.0°$	$a = 35.9$ Å $b = 71.8$ Å $c = 32.4$ Å $\alpha, \beta, \gamma = 90.0°$	$a = 38.1$ Å $b = 73.0$ Å $c = 32.5$ Å $\alpha, \beta, \gamma = 90.0°$
no. of crystals	1	1	1
wavelength (Å)	1.542	1.542	0.97954
D_{min} (Å)	1.7	1.7	2.3
R_{sym} (%)	4.3 (45.6)	4.0 (24.8)	8.0 (24.8)
completeness (%)	90.1 (98.5)	99.1 (88.1)	99.1 (93.1)
I/σ	25.6 (3.0)	138.7 (21.9)	23.2 (5.3)
phasing power			1.52
no. of observed reflections	34081	124791	
no. of unique reflections	8955	10241	
average redundancy	3.8	12.2	
residues in the structural model	6−86	5−102	
overall figure of merit	0.81	0.87	
resolution range for refinement (Å)	15.0−1.7	15.0−1.7	
R_{work} (%)	25.0	20.3	
R_{free} (%)	28.4	23.9	
average B factor (Å^2)	18.9	22.2	
no. of protein atoms	650	781	
no. of water molecules	99	144	
rmsd for bond lengths (Å)	0.0050	0.0045	
rmsd for bond angles (deg)	1.36	1.35	
rmsd for bonded B factors (Å^2)	1.38	1.30	
residues in most favored regions (%)	95.7	91.7	
residues in additional allowed regions (%)	4.3	8.3	
residues in generously allowed regions (%)	0.0	0.0	
residues in disallowed regions (%)	0.0	0.0	

[a] All X-ray data were collected at 100 K. The values in parentheses correspond to the highest-resolution shell of the X-ray data. Synchrotron data were collected at the PX beamline at the Center for Advanced Microstructures and Devices (CAMD) in Baton Rouge, LA.

1.54 Å diffraction data to a resolution of 1.7 Å. Atomic *B*-factors were refined using CNS version 1.1 (*39*). The structure of the native form of aRpp29 (which crystallized in a different space group) was determined by the molecular replacement method using CNS, with the structure of the selenomethionine form of the protein as a search model. After multiple cycles of rebuilding using omit maps, and positional and *B*-factor refinement, the structure of the native form of the protein was completed using data to a resolution of 1.7 Å. Water molecules were added to each structure where the difference electron density was greater than 3σ and the density in the $2|F_o| - |F_c|$ map was greater than 1σ. Summaries of the crystallographic and refinement statistics for the native and selenomethionine forms of the aRpp29 protein are given in Table 1. The quality and stereochemistry of the final structures were evaluated using PROCHECK (*40*). DALI (*41*) and VAST (*42*) were used to search the RCSB database for proteins that are structurally similar to aRpp29. Ribbon and stick diagrams were generated using Pymol (*43*).

NMR Spectroscopy. NMR data were collected using a 500 MHz Varian Inova spectrometer. Spectra were collected at 30 °C unless stated otherwise. The ^{1}H, ^{15}N, and ^{13}C chemical shifts for the nuclei of *A. fulgidus* aRpp29 were previously assigned using two- and three-dimensional NMR spectra as described previously (*28*). Two-dimensional (2D) ^{1}H−^{15}N correlated spectra for this work were collected using sweep widths of 8000 and 5000 Hz in the ^{1}H and ^{15}N dimensions, respectively. Data were processed using nmrPipe (*44*) and analyzed using Sparky (*45*).

Amide Proton Exchange Rate Measurements. The rates with which the backbone amide protons of the aRpp29 protein exchange with protons from the solvent were measured using a saturation-transfer method, essentially as described by Lillemoen *et al*. (*46*). Uniformly ^{15}N-labeled samples of aRpp29 were equilibrated with buffers of 10 mM K_2HPO_4/KH_2PO_4 and 100 mM NaCl at pH 5.8, 6.8, 7.8, and 8.8. A pair of ^{1}H−^{15}N correlated 2D NMR spectra was obtained at each pH. In all cases, a selective excitation method was used for water suppression. For one spectrum of each pair, the water resonance was presaturated for 3 s, resulting in attenuation of the backbone amide ^{1}H resonances due to saturation transfer from the solvent, which depends on the proton exchange rate, as well as a nuclear Overhauser effect (NOE). The NOE was assumed to be constant at each pH, while the proton exchange rate was assumed to increase 10-fold with each unit increase in pH (*47*). Via comparison of the spectra obtained with and without presaturation at each pH, the effects of solvent exchange and NOE could be determined (*46*). Amide proton exchange rates were normalized to pH 7 for comparison. Peak heights were measured for each assigned residue and fit to the equation $I_{presat}/I_o = (1 - N)/((10^{pH-7}T_1k + 1)$, where k is the amide proton exchange rate, I_{presat} and I_o are the peak heights in the ^{1}H−^{15}N correlated spectra with and without water presaturation, respectively, and N represents the NOE contribution. The longitudinal relaxation time T_1 was estimated to be 0.7 s using an inversion recovery experiment.

Alternatively, solvent exchange rates for relatively slowly exchanging amide protons were determined simply by transferring the protein to deuterated solvent and monitoring the disappearance of resonances in 2D ^{1}H−^{15}N correlated spectra, as ^{1}H is replaced with ^{2}H. A solution of uniformly ^{15}N-labeled Rpp29 was passed through a column of Sephadex

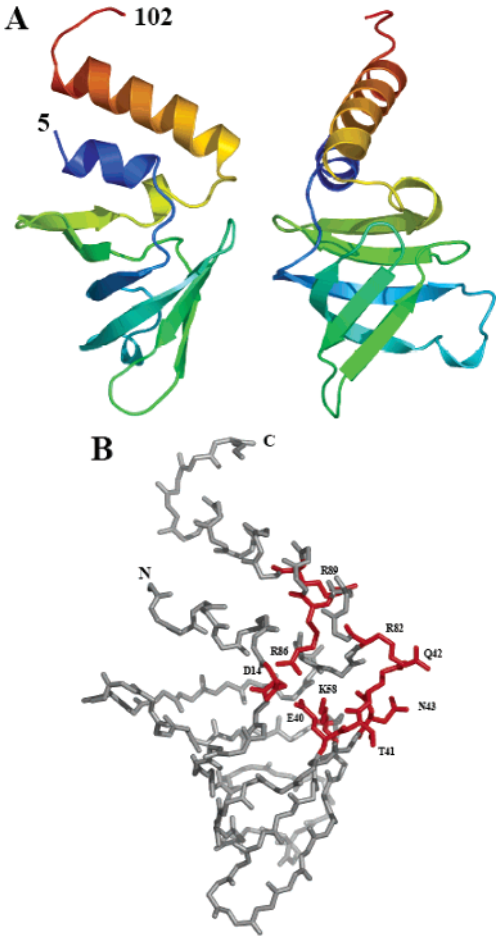

FIGURE 1: (A) Ribbon diagram showing two orthogonal views of the SeMet form of *A. fulgidus* aRpp29, color ramped from the N-terminus (blue) to the C-terminus (red). The model was generated using the backbone atoms of residues 5−102. (B) Surface residues that are conserved in a wide range of species and considered likely to interact with the RNase P RNA or other protein subunits are shown in red; these conserved residues are clustered into a relatively small region of the protein surface. Only residues 6−86 were observed in the crystal structure of the native form of the protein. This figure was created using PyMol (*41*).

G-25 beads (Sigma-Aldrich) that had been pre-equilibrated in buffer [10 mM K_2HPO_4/KH_2PO_4 (pH 5.8) and 100 mM NaCl] in 99.9% D_2O overnight. The protein was immediately placed in the NMR spectrometer, and 2D $^1H-^{15}N$ correlated spectra were collected at time intervals of 6 h over a total of 24 h, and after 48, 72, and 144 h. All spectra were processed identically using nmrPipe (*44*), and peak heights were measured using Sparky (*45*). The decrease in the peak height over time was fit to a first-order exponential decay equation. Solvent exchange rates were measured for 58 backbone amide protons; overlapping or partially overlapping peaks were not included in the analysis.

Circular Dichroism Measurements. Circular dichroism data were collected for the aRpp29 protein using an AVIV model 62DS circular dichroism spectrometer. The concentration of the protein sample was 14.2 μM in 10 mM potassium phosphate (pH 7.0) and 100 mM NaF. Data were collected at 25 °C using a cell with a path length of 1 mm. Nine scans were averaged to achieve a high signal-to-noise ratio. The parameters of each scan were as follows: wavelength range of 260−185 nm, bandwidth of 0.5 nm, and scan time of 2.0 s. The data were analyzed using Selcon3 (48).

Analytical Ultracentrifugation. Sedimentation data were collected for the *A. fulgidus* aRpp29 protein, for the purpose of determining its aggregation state in solution. Data were collected using a Beckman Coulter Optima XL-1 analytical centrifuge, operated at 20 °C with a sample concentration of 156 μM. A total of 60 UV absorbance scans were obtained at a rotor speed of 42 000 rpm, with an interval of 10 min between scans. The experiment was performed in triplicate, and data were analyzed using Ultrascan (*49*). The aRpp29 protein was found to have a sedimentation coefficient of 1.25 ± 0.06 S at 20 °C in the same buffer that was used for the NMR experiments [100 mM NaCl and 10 mM K_2HPO_4/KH_2PO_4 (pH 5.8)]; for comparison, hen egg white lysozyme, with 129 amino acids, was found to have a sedimentation coefficient that is slightly greater (1.60 ± 0.04 S) under these same conditions. These sedimentation data are most consistent with aRpp29 being a monomer in solution.

RESULTS

Crystal Structure of A. fulgidus aRpp29. Crystals of the *A. fulgidus* aRpp29 protein were grown from a solution of sodium citrate with ammonium sulfate as the precipitant; the crystals formed in space group $P2_12_12_1$ and diffract X-rays to 1.7 Å resolution. A derivative of aRpp29 containing selenomethionine (SeMet) in place of methionine was prepared as a tool for solving the phase problem by anomalous scattering methods. Interestingly, the SeMet-containing aRpp29 did not crystallize under the same conditions as the native form of the protein. However, crystals with a slightly larger unit cell diffracting to 1.7 Å were obtained in space group $P2_12_12$ from a solution of HEPES and ammonium sulfate. Obtaining two different crystal forms of aRpp29 was fortuitous in that it provided for two independent views of the protein structure. Several of the methionine residues were found to be located on the intermolecular contacts within the crystal, thus providing an explanation for the change in molecular packing upon substituting selenomethionine for methionine.

The electron density maps for each crystal form of aRpp29 were of excellent quality. For the SeMet form of the protein, residues 5−102 were built into the maps and refined; amino acids 1−4 were disordered and could not be confidently built into the structure. For the native protein, only residues 6−86 were clearly observed in the electron density maps; inspection of the molecular packing suggests that the C-terminal residues were absent in the native form of the protein, presumably due to degradation prior to crystallization. This observation is consistent with the significant difference in crystallization time for the two crystal forms. The SeMet protein crystallizes in several days, while the native protein requires 2 months to form crystals. The native and SeMet structures were refined to 1.7 Å with $R_{working}$ values of 25.0 and 20.3% and R_{free} values of 28.4 and 23.9%, respectively. The solvent contents of 31.7 and 30.2% (v/v) for the native and SeMet crystal forms, respectively, are at the lower end of the range typical for protein crystals; this is consistent with relatively tight packing of the protein molecules and excellent diffraction. The two structures can be superimposed with an rmsd of 0.8 Å for the C_α atoms, with most of the variation coming from the last few residues at the C-terminus. Both structures have been deposited to the Protein Data Bank (entries 1TS9 and 1TSF).

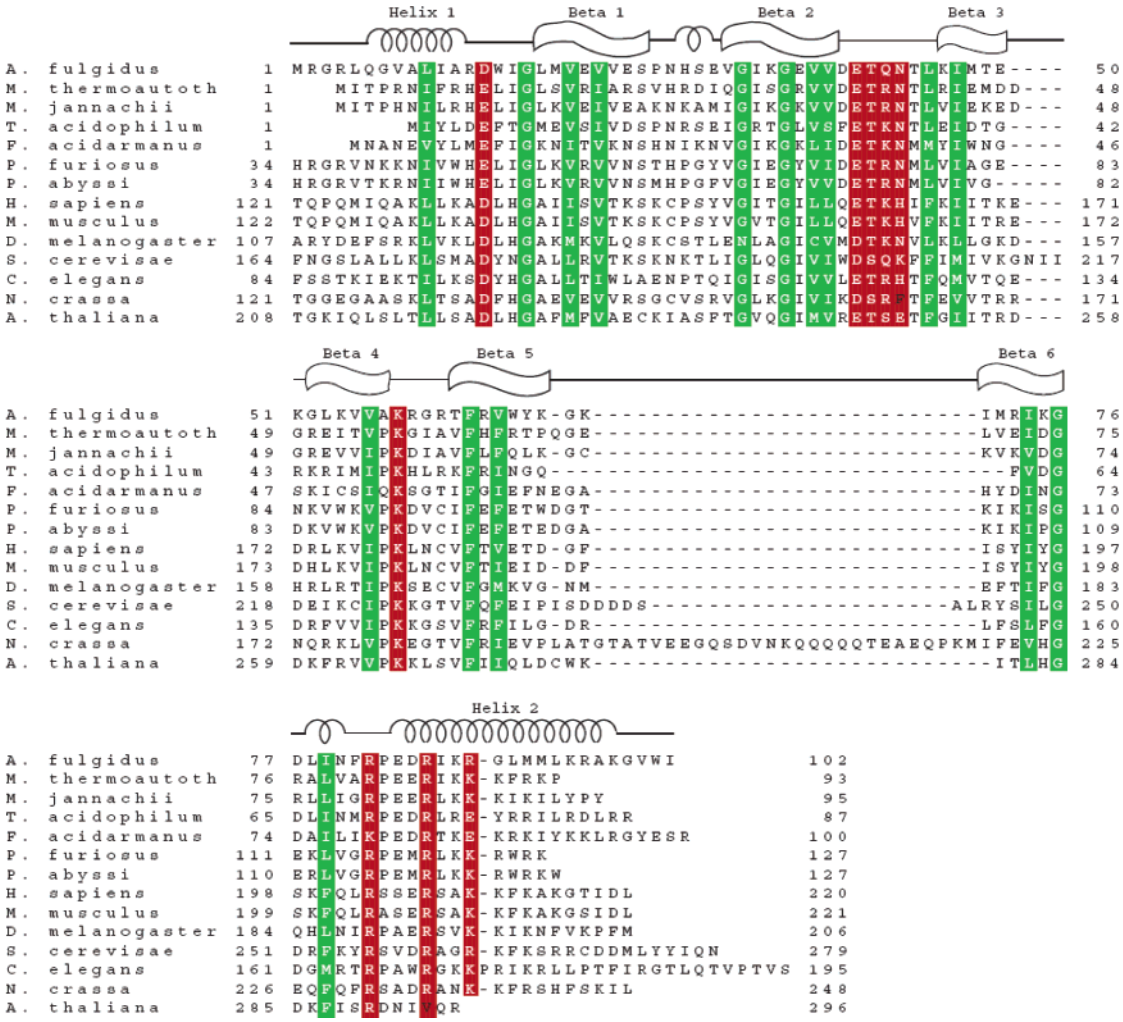

FIGURE 2: Amino acid sequence alignment of *A. fulgidus* aRpp29 and RNase P proteins from other archaea and eukarya. Sequences from seven archaeal species are shown: *Archaeoglobus fulgidus Methanococcus thermoautotrophicus*, *Methanococcus jannaschii*, *Thermoplasma acidophilum*, *Ferroplasma acidarmanus*, *Pyrococcus furiosus*, and *Pyrococcus abyssi*. The eukaryotic sequences are from *Homo sapiens*, *Mus musculus*, *Drosophila melanogaster*, *Saccharomyces cerevisae*, *Caenorhabditis elegans*, *Neurospora crassa*, and *Arabidopsis thaliana*. Archaeal aRpp29 is homologous to the C-terminal half of eukaryotic Rpp29. The N-terminal region of Rpp29 is not well conserved among eukarya. The most conserved hydrophobic residues, which form the hydrophobic core of aRpp29, are boxed in green. The conservation of these residues suggests that the fold is conserved across the wide range of species shown. Conserved surface residues that are most likely to be involved in mediating protein−RNA or protein−protein interactions within RNase P are boxed in red.

The central feature of the aRpp29 protein is a sheet of six antiparallel β-strands formed by residues 17−75; this β-sheet is significantly twisted and wrapped around a core of conserved hydrophobic amino acids [Val20, Val22, Val37, Val38, Leu45, Ile47, Val56, Phe63, Val65, and Ile74 (Figure 1)]. The high degree of conservation of these hydrophobic residues in the archaeal aRpp29, yeast Pop4, and human Rpp29 indicates that each of these proteins contains a similar β-sheet structure (Figure 2). Within the β-sheet, strand β1 is connected to β2 by a seven-residue loop containing one turn of helix centered at residue 28, and strand β2 is connected to β3 by a short loop, as is β3 to β4. Strand β4 is connected to β5, located at the opposite side of the protein, by a five-residue loop that spans the open part of the twisted β-sheet. Strand β5 is connected to β6 by a compact turn, followed by a seven-residue loop containing one turn of helix centered at residue 76.

The N-terminal region of the aRpp29 protein contains a two-turn α-helix (residues 6−12), followed by a short loop leading to the first β-strand. Side chains of residues Leu10, Ile11, and Trp15 are oriented toward the hydrophobic face of the β-sheet; residues at these positions are hydrophobic in aRpp29 from most species, suggesting that the N-terminal helix is a conserved feature of the protein structure. The C-terminal region of the SeMet form of the protein contains a four-turn α-helix formed by residues 83−96, followed by an irregular loop to residue Trp101. In the native form of the protein, only a single turn of this helix is observed in the electron density map. The N- and C-terminal helices are aligned antiparallel to each other, which may be a stabilizing feature since it provides for a favorable alignment of the helix dipoles. In the SeMet form of the protein, the N- and C-terminal helices make intermolecular contacts near a 2-fold axis within the crystal. The selenomethionine residues are all exposed on the protein surface, with SeMet19, -48, and -92 being directly involved in forming crystal contacts. In contrast, the packing of the native protein is mediated by the N-terminal helix and the C-terminal region from Asp77 to Arg86 packing against the surface of the β-sheet formed by strands β1, β2, β5, and β6.

Conserved Surface Residues of aRpp29. Amino acids are generally conserved among homologous proteins from a

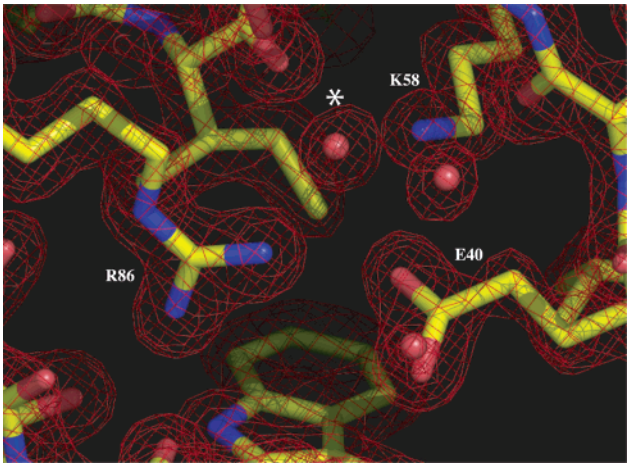

FIGURE 3: Region of $2|F_o| - |F_c|$ electron density map from the aRpp29 crystal structure showing the internal salt bridge formed by the triad of Glu40, Lys58, and Arg86. These residues are nearly completely inaccessible to the solvent. The distances from Glu40 Oϵ to Lys58 Nζ and Glu40 Oϵ to Arg86 Nη are 2.71 and 2.63 Å, respectively. The water molecule marked with an asterisk is involved in mediating the interaction between Lys58 and Arg86; the oxygen of this water molecule is 3.10 Å from Lys58 Nζ and 2.94 Å from Arg86 Nη. The map is contoured at 1.5σ. This figure was created with PyMol (*41*).

diverse set of species when they are important for purposes of structure, function, or intermolecular interactions. In the case of aRpp29 and its homologues (Figure 2), conserved hydrophobic residues in the protein core are likely to be essential for stabilizing the overall protein fold. The conserved residues on the protein surface are the most likely to be important for intermolecular interactions, such as contacting the RNase P RNA or other protein components. The most conserved residues on the surface of aRpp29 are spread throughout the primary sequence of the protein, but are spatially clustered into a single region of the protein surface (Figure 1B). Six surface residues (Asp14, Thr41, Gln42, Asn43, Arg82, and Arg88) that are well-conserved in archaeal aRpp29, as well as the RNase P proteins Rpp29 and Pop4 in eukarya, are located either within or near the loop connecting strands β2 and β3, and the beginning of helix α2 (Figures 1 and 2). Each of these six conserved surface residues may act as either a hydrogen bond donor or acceptor, and is potentially a site of interaction with the RNase P RNA, the substrate pre-tRNA, or both. Another interesting feature of the protein is a salt bridge formed by the triad of residues Glu40, Lys58, and Arg86 (Figure 3). These hydrophilic amino acid types are most commonly found on the surface of proteins; however, in aRpp29, the charged ends of these residues are buried so that the salt bridge spans an interior region of the protein. This triad of residues is conserved from aRpp29 in *A. fulgidus* to Rpp29 in humans and Pop4 in yeast.

The alignment of the aRpp29 sequence with sequences of homologous proteins (Figure 2) indicates that one of the most conserved residues is a glycine (Gly35 in *A. fulgidus* aRpp29) located at a bend near the center of strand β2. A Ramachandran plot for aRpp29 shows that Gly35 has ϕ and ψ angles that would be unfavorable for any other amino acid type (163° and −169°, respectively). This glycine therefore appears to be essential to the fold of the protein, in that it allows the structure to form its strongly bent open barrel.

Comparison of the Crystal and Solution Structures of aRpp29. The solution structures of aRpp29 from two species of archaea (*A. fulgidus* and *M. thermoautotrophicus*) have recently been determined using NMR methods (*28*, *29*). The crystal and NMR structures are similar in that each method describes essentially the same six-stranded antiparallel twisted β-sheet (Figure 4), and the large majority of NMR-derived interproton distances are consistent with the crystal structure. Indeed, the NMR structure of *A. fulgidus* aRpp29 (*28*) identified exactly the same set of hydrogen bonds connecting the antiparallel strands that is observed here in the crystal. On the other hand, there are immediately obvious differences between the crystal and solution structures (Figure 4). Most notably, the well-ordered helices at the N- and C-termini of the protein in the crystal are not observed in solution, even upon re-examination of the NMR data in view of the crystallography results. NMR chemical shift index values for the residues of the C-terminal helix provided a hint of helical structure in solution; however, the ^{1}H−^{1}H NOE cross-peaks typical of helical structure were not observed for either the N-terminal or C-terminal helix (*28*). The rmsd between the backbone atoms of residues 18−76 of the crystal and NMR structures of the *A. fulgidus* protein exceeds 3 Å, which is larger than the likely uncertainty in the structures, suggesting that there likely are some real differences in the overall twist of the β-sheet. Several observed NOE cross-peaks involving loop residues (particularly Ser25) are inconsistent with distances in the crystal structure, indicating there are some differences in the loop structures of the solution and crystalline forms of the protein. In addition, the internal three-way salt bridge among residues Glu40, Lys58, and Arg86 in the crystal (Figure 3) was not observed in the solution structures of either archaeal protein, although the salt bridge between two residues of this triad (Glu40−Lys58) was detected in the *M. thermoautotrophicus* solution structure (*29*).

The apparent differences between the crystal and NMR structures suggest that the crystallization process may lead to a "freezing-out" of a single ordered form of the molecule, and that in solution the helices at the N- and C-termini of the protein may be in equilibrium between folded and unfolded forms. The biophysical tools of NMR and circular dichroism provide additional means of testing this hypothesis, and reconcile the apparent differences between the crystal and solution structures of aRpp29. Understanding these differences is important since a simple static model of the structure may not provide an accurate description of the protein surface; a detailed understanding of the protein surface may be required to identify which residues make the essential intersubunit and enzyme−substrate interactions within RNase P.

Reconciling Differences between the Crystal and Solution Structures of aRpp29. The large majority of the helical content within the crystal structure of aRpp29 resides in the N- and C-terminal helices; the helical content of the crystal structure is approximately 28%. Circular dichroism (CD) measurements provide information from which the helical content of aRpp29 can be estimated in solution. CD data from *A. fulgidus* aRpp29 collected at 25 °C were analyzed using Selcon3 (*49*), indicating a helical content of 7.4% in solution; other methods of CD data analysis indicated a helical content of 5−12%. The CD data therefore indicate

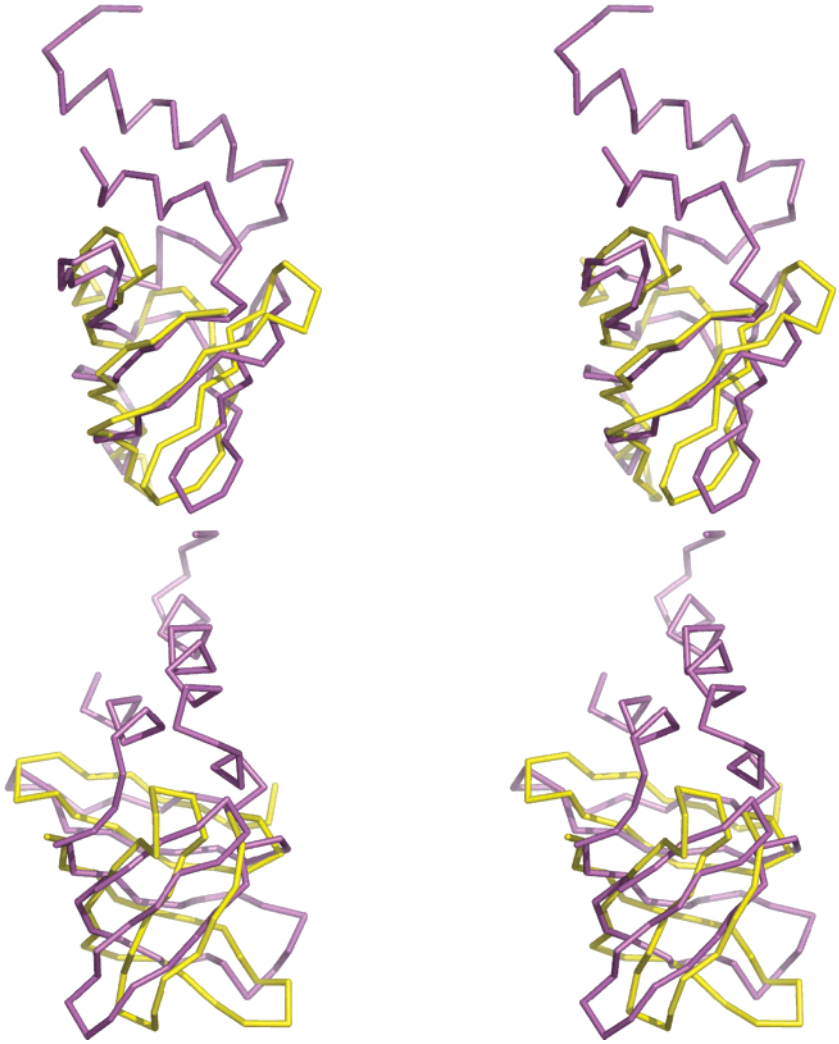

FIGURE 4: Stereodiagram showing two orthogonal views of the *A. fulgidus* aRpp29 NMR structure superimposed onto the crystal structure. The backbone atoms of the NMR model (yellow), consisting of residues 17−77, were superimposed on the backbone atoms of the crystal structure (pink) with an rmsd of 3.7 Å. The main difference between the crystal and NMR structures is in the orientation of strands β1, β2, and β5 of the β-sheet, which appears to be slightly rotated when the structures are compared. This figure was created using PyMol (*41*).

that the helical content of aRpp29 in solution is approximately one-third of that in the crystal. The CD data are consistent with either (1) approximately two-thirds of the helical structure of aRpp29 being unfolded in solution or (2) the helices of aRpp29 existing in equilibrium between folded and unfolded states, with the equilibrium slightly favoring the unfolded form.

While circular dichroism measurements provide information regarding the average helical content of aRpp29 in solution, measurements of the rates at which backbone amide protons exchange with the solvent can provide insight into how frequently the helices unfold. Amide protons along the protein backbone are only competent to exchange with the solvent when they are not involved in stable hydrogen bonds. Thus, the frequency with which a proton exchanges with solvent sets an upper limit on how frequently a hydrogen bond opens. The solvent exchange rates for the backbone amide protons of aRpp29 were measured using NMR methods. Slowly exchanging amide protons were monitored by simply observing the decay of ^{1}H NMR signals after the protein is transferred to deuterated solvent, while rates of rapidly exchanging protons were measured using a saturation transfer method (Figure 5). Amide proton exchange rates in aRpp29 were found to range over several orders of magnitude. Amide protons within the central regions of the antiparallel β-sheet were found to have exchange rates of less than 10^{-4} s^{-1} at pH 7, consistent with being in a stable hydrogen-bonded structure that opens infrequently. In contrast, the exchange rates for amide protons of the residues of the N- and C-terminal helices are several orders of magnitide more rapid. For example, solvent exchange rates of amide protons of Lys88 and Gly90, located in the middle of C-terminal helix α2 in the crystal structure, are approximately 1.0 s^{-1}, indicating that these hydrogen bonds open much more frequently than those in the β-sheet. For the residues of N-terminal helix α1, the backbone amide protons exchanged with the solvent too rapidly for measurement by the saturation transfer method, or were altogether unobservable due to rapid exchange.

In summary, CD and NMR data support a model in which the N- and C-terminal helices that are clearly observed in the crystal structure of *A. fulgidus* aRpp29 either are unfolded in solution or are in rapid equilibrium between folded and unfolded states. These observations are consistent with our previously reported measurements of ^{15}N NMR relaxation rates (an alternative method of identifying flexible regions

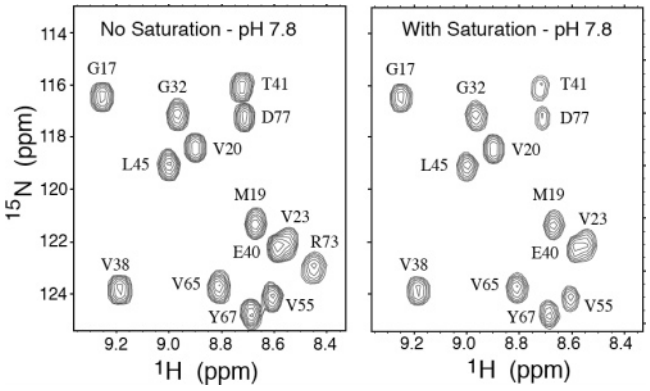

FIGURE 5: Analysis of rates of saturation transfer between solvent water and amide protons can be used to gain insight into the motions within the Rpp29 protein. (A) A section of the $^{15}N-^{1}H$ correlated NMR spectrum of Rpp29 obtained using a selective excitation method for solvent suppression. (B) A spectrum obtained under the same conditions, but in this case saturating the solvent water resonance. NMR signals from amide protons involved in stable hydrogen bonds are relatively uninfluenced by saturating the solvent resonance. In contrast, signals from amide protons that exchange with protons from the solvent during the saturation period are significantly reduced in intensity; examples are Thr41 and Asp77, which are partially attenuated, and Arg73, at the bottom right, which is completely attenuated when the water resonance is saturated. The influence of the nuclear Overhauser effect is separated from that of amide exchange by performing the experiment at several different pH values.

within a protein structure), which indicated that the residues of the β-sheet for *A. fulgidus* aRpp29 are significantly less mobile in solution than those of the termini (*28*).

DISCUSSION

Of the four known archaeal RNase P proteins (*10*), two now have had their three-dimensional structures determined: *A. fulgidus* aRpp29 (homologous to yeast Pop4 and human Rpp29) described in this work and RNase P protein Ph1887p from *Pyrococcus horikoshii* (*29*), which is a homologue of eukaryotic RNase P proteins Rpp30 in yeast and Rpp1 in humans. Amino acid sequence comparisons support the view that there is a structural (and presumably evolutionary) relationship between the proteins of the archaeal and eukaryotic RNase P. Neither of the archaeal RNase P proteins with known structure shows any similarity to the bacterial RNase P protein, which has been characterized by both crystallographic and NMR methods (*25*−*27*). Interestingly, when RNA components are compared, the archaeal RNase P appears to be more similar to that of bacteria than that of eukarya (*4*, *6*, *50*). At this point, structural results as well as sequence comparisons seem to indicate that the archaeal RNase P contains a mixture of bacterial and eukaryotic features.

The results of this work show that there are clear differences between the crystal and solution structures of *A. fulgidus* RNase P protein aRpp29, with the most obvious differences being the existence of the ordered N- and C-terminal helices in the crystal; studies by us and others indicate that the residues that form these helices are relatively mobile in solution (*28*, *29*). The crystallographic *B*-factors for backbone atoms of the N- and C-terminal helices are 24 and 15 Å^2, respectively, consistent with well-ordered structures. This raises the question of whether the N- and C-terminal helices are simply interesting crystallization artifacts, and biologically irrelevant. Several observations argue for the significance of the helices. An extremely well-conserved hydrophobic amino acid is located at the center of the N-terminal helix (Leu10 in the *A. fulgidus* sequence), with its side chain extending into the hydrophobic core of the twisted β-sheet; this interaction appears to fix and stabilize the contact between the N-terminal helix and the core of the protein. If the N-terminal helix was unnecessary or absent, there would not be any reason for the conservation of Leu10. The hydrophobic nature of Leu10 is conserved over a wide range of species, from archaea to humans (Figure 2), suggesting that the ability of the N-terminal residues to form a helical structure is retained, and is perhaps quite important. The side chain of Trp15 is oriented toward the core of the protein and conserved as hydrophobic over a wide range of species, suggesting that the structure of the loop connecting the N-terminal helix with strand β1 is also conserved. The presence of an essentially identical N-terminal helix in the two different crystal forms (native and SeMet) of aRpp29 also suggests that it is more than simply a crystallization artifact. There do not appear to be any well-conserved hydrophobic contacts stabilizing the C-terminal helix (Figure 2); the full length of this helix is only observed in the crystal structure of the SeMet form of the protein. The crystal structure of the *P. horikoshii* homologue of aRpp29 was very recently reported (*31*), and found to be similar to the crystal structure of *A. fulgidus* aRpp29 described here, with the N- and C-terminal helices being present. Interestingly, the large ribosomal subunit provides several examples of proteins with termini that are flexible in solution yet form extended and ordered RNA contacts in the crystal (*22*). Whether the termini of aRpp29 are helical or extended when the protein is in the context of the complete and intact RNase P remains an open question.

A particularly interesting feature of the aRpp29 structure is the internal salt bridge involving the triad of residues Glu40, Lys58, and Arg86 and two buried water molecules (Figure 3). A study of salt bridges within protein structures indicates that such a three-way internal structure is rather unusual (*51*), and the degree to which the identity of each of these residues is conserved is also quite striking (Figure 2). It seems to be reasonable to speculate that the residues of the salt bridge are conserved for a reason. One possibility is that the salt bridge is required simply for protein stability. However, this study provides evidence that the N- and C-terminal helices are far from rigidly stable, suggesting that the salt bridge is often not as buried as it appears to be in the crystal. Also, the observation that these residues are conserved not just in thermophilic archaea but also in higher eukarya raises the possibility that they may have important roles in the context of the RNase P ribonucleoprotein complex.

The results of this work show that aRpp29 is structurally similar to the Sm and Sm-like (Lsm) proteins. The Sm fold is defined by an N-terminal helix followed by a five-stranded antiparallel β-sheet that forms an open barrel (*50*). The structure of aRpp29 is therefore a variation of this fold, as it contains the N-terminal helix and five β-strands (β1−β5) exhibiting the same connectivity, with strand β6 and the C-terminal helix being extra elements. The Sm-like proteins occur in all three domains of life (bacteria, archaea, and

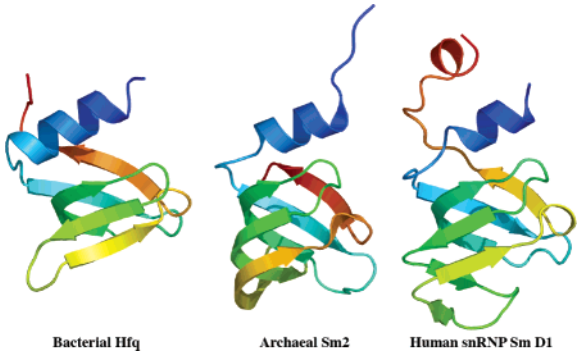

FIGURE 6: Cartoon representations of proteins that are similar in structure to aRpp29 and exhibit the Sm fold, demonstrating its conservation across all three domains of life. The diagrams are color ramped from blue at the N-terminus to red at the C-terminus. The proteins shown are Host-factor q (Hfq) from *E. coli* (PDB entry 1HK9), an RNA-binding protein involved in regulating translation; Sm-2 from *A. fulgidus* (PDB entry 1LJO); and Sm-D1 from *H. sapiens* (PDB entry 1B34), which forms a dimer with Sm-D2 and interacts with the 3′-terminal U-tract of U6 snRNA. The rmsds between the backbone atoms of *A. fulgidus* aRpp29 (residues 17−77) and Hfq, Sm2, and Sm-D1 are 2.2, 2.1, and 3.5 Å, respectively. This figure was created using PyMol (*41*).

eukarya), and are known to associate with U-rich RNA sequences. Sm and Sm-like proteins are known to be involved in a variety of RNA processing events, including pre-mRNA splicing (*53*) and the biogenesis of the small nuclear ribonucleoprotein particles (snRNPs), as well as interaction with pre-RNase P RNA (*54*; reviewed in ref *55*).

The structural similarity between the β-sheet regions of aRpp29 and the Sm-like protein and bacterial transcription factor Hfq (*56*) was noted in our previous NMR study (*28*); however, the similarity between these proteins becomes even more apparent now that the crystal structure of aRpp29 is known, since Hfq contains a helix that corresponds to the N-terminal helix of aRpp29. In addition to their structural similarity, there is a slight but detectable amino acid sequence similarity between aRpp29 and Hfq. The bacterial Hfq protein contains the glycine at the bend in the central region of strand β2 (corresponding to the well-conserved Gly35 in *A. fulgidus* aRpp29) that appears to be essential for forming the characteristically bent β-sheet. The similarity between aRpp29 and other Sm family members is not always noticeable at the level of primary sequence, although the structural similarity is fairly obvious. Unlike the apparently monomeric aRpp29, many of the Sm-like proteins form hexameric or heptameric complexes (*52*, *56*, *57*; reviewed in ref *58*). The structural similarity to aRpp29 can be seen in the ribbon diagrams of the monomer units of Sm and Sm-like proteins Hfq, Sm2, and human snRNP D1 shown in Figure 6.

The structure of a complex of Hfq with a single-stranded oligoribonucleotide (*56*) shows that the RNA binds in a basic cleft; however, the residues of Hfq that contact the RNA do not correspond to conserved residues in aRpp29, suggesting that the RNA binding modes of these proteins are different. An NMR chemical shift perturbation study of the *M. thermoautotrophicus* homologue of aRpp29 by Boomershine *et al*. (*29*) suggested that a broad surface involving a number of the β-sheet residues may contact the RNA, which differs from the conserved surface that we suggest in Figure 1B. In the recently published crystal structure of the *P. horikoshii* homologue of aRpp29, Numata *et al*. (*31*) propose a concave surface near the β2−β3 connecting loop as a possible site of interaction with RNA. The *A. fulgidus* aRpp29 as a whole is a basic protein, and conserved basic residues such as Arg82 and Arg89 on the protein surface (Figure 2B) are likely candidates for RNA contacts; however, an electrostatic surface plot based on this crystallographic work does not indicate any single surface that is overwhelmingly positive in charge. It appears to be clear that structural results for an aRpp29 protein−RNA complex will be required before the details of the protein−RNA interaction are understood.

Although the details of the interactions between aRpp29 and the other RNase P components remain unknown, it seems likely that aRpp29 is central to the overall structure. Pieces of evidence that support this speculation include interaction maps derived from two- and three-hybrid assays that indicate the yeast and human homologues of aRpp29 contact other RNase P proteins as well as the eukaryotic RNase P RNA (*9*, *32*), and the recent observation that the eukaryotic homologue of the Rpp29 protein and the *E. coli* RNase P RNA by themselves form a complex with catalytic activity (*33*). The high-resolution model of the aRpp29 protein provided by this work, and the identification of a well-conserved protein surface likely to participate in intersubunit interactions, are essential steps toward improving our understanding of the overall architecture of RNase P.

ACKNOWLEDGMENT

The authors thank Dr. Xiaohua Chen of the Department of Biochemistry and Biophysics at Texas A&M University for her help in acquiring the circular dichroism spectra.

REFERENCES

1. Robertson, H. D., Altman, S., and Smith, J. D. (1972) Purification and properties of a specific *Escherichia coli* ribonuclease which cleaves a tyrosine transfer ribonucleic acid presursor, *J. Biol. Chem. 247*, 5243−5251.
2. Frank, D. N., and Pace, N. R. (1998) Ribonuclease P: unity and diversity in a tRNA processing ribozyme, *Annu. Rev. Biochem. 67*, 153−180.
3. Schön, A. (1999) Ribonuclease P: The diversity of a ubiquitous RNA processing enzyme, *FEMS Microbiol. Rev. 23*, 391−406.
4. Brown, J. W. (1999) The Ribonuclease P Database, *Nucleic Acids Res. 27*, 314.
5. Guerrier-Takada, C., Gardiner, K., Marsh, T., Pace, N., and Altman, S. (1983) The RNA moiety of ribonuclease P is the catalytic subunit of the enzyme, *Cell 35*, 849−857.
6. Pannucci, J. A., Haas, E. S., Hall, T. A., Harris, J. K., and Brown, J. W. (1999) RNase P RNAs from some Archaea are catalytically active, *Proc. Natl. Acad. Sci. U.S.A. 96*, 7803−7808.
7. Kurz, J. C., Niranjanakumari, S., and Fierke, C. A. (1998) Protein component of *Bacillus subtilis* RNase P specifically enhances the affinity for precursor-tRNAAsp, *Biochemistry 37*, 2393−2400.
8. Jarrous, N., and Altman, S. (2001) Human ribonuclease P, *Methods Enzymol. 342*, 93−100.
9. Houser-Scott, F., Xiao, S., Millikin, C. E., Zengel, J. M., Lindahl, L., and Engelke, D. R. (2002) Interactions among the protein and RNA subunits of *Saccharomyces cerevisiae* nuclear RNase P, *Proc. Natl. Acad. Sci. U.S.A. 99*, 2684−2689.
10. Hall, T. A., and Brown, J. W. (2002) Archaeal RNase P has multiple protein subunits homologous to eukaryotic nuclear RNase P proteins, *RNA 8*, 296−306.
11. Kouzuma, Y., Mizoguchi, M., Takagi, H., Fukuhara, H., Tsukamoto, M., Numata, T., and Kimura, M. (2003) Reconstitution of archaeal ribonuclease P from RNA and four protein components, *Biochem. Biophys. Res. Commun. 306*, 666−673.

12. Andrews, A. J., Hall, T. A., and Brown, J. W. (2001) Characterization of RNase P holoenzymes from *Methanococcus jannaschii* and *Methanothermobacter thermoautotrophicus*, *Biol. Chem. 382*, 1171−1177.
13. Hartmann, E., and Hartmann, R. K. (2003) The enigma of ribonuclease P evolution, *Trends Genet. 19*, 561−569.
14. Hsieh, J., Andrews, A. J., and Fierke, C. A. (2004) Roles of protein subunits in RNA-protein complexes: lessons from ribonuclease P, *Biopolymers 73*, 79−89.
15. Pley, H. W., Flaherty, K. M., and McKay, D. B. (1994) Three-dimensional structure of a hammerhead ribozyme, *Nature 372*, 68−74.
16. Scott, W. G., Murray, J. B., Arnold, J. R., Stoddard, B. L., and Klug, A. (1996) Capturing the structure of a catalytic RNA intermediate: the hammerhead ribozyme, *Science 274*, 2065−2069.
17. Ferre-D'Amare, A. R., Zhou, K., and Doudna, J. A. (1998) Crystal structure of a hepatitis delta virus ribozyme, *Nature 395*, 567−574.
18. Ke, A., Zhou, K., Ding, F., Cate, J. H., and Doudna, J. A. (2004) A conformational switch controls hepatitis delta virus ribozyme catalysis, *Nature 429*, 201−205.
19. Cate, J. H., Gooding, A. R., Podell, E., Zhou, K., Golden, B. L., Kundrot, C. E., Cech, T. R., and Doudna, J. A. (1996) Crystal structure of a group I ribozyme domain: principles of RNA packing, *Science 273*, 1678−1685.
20. Wedekind, J. E., and McKay, D. B. (2003) Crystal structure of the leadzyme at 1.8 Å resolution: metal ion binding and the implications for catalytic mechanism and allo site ion regulation, *Biochemistry 42*, 9554−9563.
21. Wimberly, B. T., Brodersen, D. E., Clemons, W. M., Jr., Morgan-Warren, R. J., Carter, A. P., Vonrhein, C., Hartsch, T., and Ramakrishnan, V. (2000) Structure of the 30S ribosomal subunit, *Nature 407*, 327−339.
22. Ban, N., Nissen, P., Hansen, J., Moore, P. B., and Steitz, T. A. (2000) The complete atomic structure of the large ribosomal subunit at 2.4 Å resolution, *Science 289*, 905−920.
23. Krasilnikov, A. S., Yang, X., Pan, T., and Mondragon, A. (2003) Crystal structure of the specificity domain of ribonuclease P, *Nature 421*, 760−764.
24. Tsai, H. Y., Masquida, B., Biswas, R., Westhof, E., and Gopalan, V. (2003) Molecular modeling of the three-dimensional structure of the bacterial RNase P holoenzyme, *J. Mol. Biol. 325*, 661−675.
25. Spitzfaden, C., Nicholson, N., Jones, J. J., Guth, S., Lehr, R., Prescott, C. D., Hegg, L. A., and Eggleston, D. S. (2000) The structure of ribonuclease P protein from *Staphylococcus aureus* reveals a unique binding site for single-stranded RNA, *J. Mol. Biol. 295*, 105−115.
26. Stams, T., Niranjanakumari, S., Fierke, C. A., and Christianson, D. W. (1998) Ribonuclease P protein structure: evolutionary origins in the translational apparatus, *Science 280*, 752−755.
27. Kazantsev, A. V., Krivenko, A. A., Harrington, D. J., Carter, R. J., Holbrook, S. R., Adams, P. D., and Pace, N. R. (2003) High-resolution structure of RNase P protein from *Thermotoga maritima*, *Proc. Natl. Acad. Sci. U.S.A. 100*, 7497−7502.
28. Sidote, D. J., and Hoffman, D. W. (2003) NMR structure of an archaeal homologue of ribonuclease P protein Rpp29, *Biochemistry 42*, 13541−13550.
29. Boomershine, W. P., McElroy, C. A., Tsai, H. Y., Wilson, R. C., Gopalan, V., and Foster, M. P. (2003) Structure of Mth11/Mth Rpp29, an essential protein subunit of archaeal and eukaryotic RNase P, *Proc. Natl. Acad. Sci. U.S.A. 100*, 15398−15403.
30. Takagi, H., Watanabe, M., Kakuta, Y., Kamachi, R., Numata, T., Tanaka, I., and Kimura, M. (2004) Crystal structure of the ribonuclease P protein Ph1877p from hyperthermophilic archaeon *Pyrococcus horikoshii* OT3, *Biochem. Biophys. Res. Commun. 319*, 787−794.
31. Numata, T., Ishimatsu, I., Kakuta, Y., Tanaka, I., and Kimura, M. (2004) Structure of archaeal ribonuclease P protein Ph1771p from *Pyrococcus horikoshii* OT3: An archaeal homolog of eukaryotic ribonuclease P protein Rpp29, *RNA 10*, 1423−1432.
32. Jiang, T., and Altman, S. (2001) Protein−protein interactions with subunits of human nuclear RNase P, *Proc. Natl. Acad. Sci. U.S.A. 98*, 920−925.
33. Mann, H., Ben-Asouli, Y., Schein, A., Moussa, S., and Jarrous, N. (2003) Eukaryotic RNase P: role of RNA and protein subunits of a primordial catalytic ribonucleoprotein in RNA-based catalysis, *Mol. Cell 12*, 925−935.
34. Van Duyne, G. D., Standaert, R. F., Karplus, P. A., Schreiber, S. L., and Clardy, J. (1993) Atomic structures of the human immunophilin FKBP-12 complexes with FK506 and rapamycin, *J. Mol. Biol. 229*, 105−124.
35. Otwinowski, Z., and Minor, W. (1997) Procesing of X-ray Diffraction Data Collected in Oscillation Mode, *Methods Enzymol. 276*, 307−326.
36. Bricogne, G., Vonrhein, C., Flensburg, C., Schiltz, M., and Paciorek, W. (2003) Generation, representation and flow of phase information in structure determination: recent developments in and around SHARP 2.0, *Acta Crystallogr. D59*, 2023−2030.
37. Perrakis, A., Harkiolaki, M., Wilson, K. S., and Lamzin, V. S. (2001) ARP/wARP and molecular replacement, *Acta Crystallogr. D57*, 1445−1450.
38. McRee, D. E. (1999) XtalView/Xfit: A versatile program for manipulating atomic coordinates and electron density, *J. Struct. Biol. 125*, 156−165.
39. Brünger, A. T., Adams, P. D., Clore, G. M., DeLano, W. L., Gros, P., Grosse-Kunstleve, R. W., Jiang, J. S., Kuszewski, J., Nilges, M., Pannu, N. S., Read, R. J., Rice, L. M., Simonson, T., and Warren, G. L. (1998) Crystallography & NMR system: A new software suite for macromolecular structure determination, *Acta Crystallogr. D54* (Part 5), 905−921.
40. Laskowski, R. A., Rullmannn, J. A., MacArthur, M. W., Kaptein, R., and Thornton, J. M. (1996) AQUA and PROCHECK-NMR: programs for checking the quality of protein structures solved by NMR, *J. Biomol. NMR 8*, 477−486.
41. Holm, L., and Sander, C. (1993) Protein structure comparison by alignment of distance matrices, *J. Mol. Biol. 233*, 123−138.
42. Gibrat, J. F., Madej, T., and Bryant, S. H. (1996) Surprising similarities in structure comparison, *Curr. Opin. Struct. Biol. 6*, 377−385.
43. DeLano, W. L. (2002) The PyMol Molecular Graphics System, DeLano Scientific, San Carlos, CA.
44. Delaglio, F., Grzesiek, S., Vuister, G. W., Zhu, G., Pfeifer, J., and Bax, A. (1995) NMRPipe: a multidimensional spectral processing system based on UNIX pipes, *J. Biomol. NMR 6*, 277−293.
45. Goddard, T. D., and Kneller, D. G. (2002) *Sparky 3*, University of California, San Francisco.
46. Lillemoen, J., Cameron, C. S., and Hoffman, D. W. (1997) The stability and dynamics of ribosomal protein L9: investigations of a molecular strut by amide proton exchange and circular dichroism, *J. Mol. Biol. 268*, 482−493.
47. Spera, S., Ikura, M., and Bax, A. (1991) Measurement of the exchange rates of rapidly exchanging amide protons: application of calmodulin and its complex with a myosin light chain kinase fragment, *J. Biomol. NMR 1*, 155−165.
48. Sreerama, N., Venyaminov, S. Y., and Woody, R. W. (2000) Estimation of protein secondary structure from circular dichroism spectra: inclusion of denatured proteins with native proteins in the analysis, *Anal. Biochem. 287*, 243−251.
49. Demeler, B., Saber, H., and Hansen, J. C. (1997) Identification and Interpretation of Complexity in Sedimentation Velocity Boundaries, *Biophys. J. 72*, 397−407.
50. Harris, J. K., Haas, E. S., Williams, D., Frank, D. N., and Brown, J. W. (2001) New insight into RNase P RNA structure from comparative analysis of the archaeal RNA, *RNA 7*, 220−232.
51. Kumar, S., and Nussinov, R. (1999) Salt bridge stability in monomeric proteins, *J. Mol. Biol. 293*, 1241−1255.
52. Toro, I., Basquin, J., Teo-Dreher, H., and Suck, D. (2002) Archaeal Sm proteins form heptameric and hexameric complexes: crystal structures of the Sm1 and Sm2 proteins from the hyperthermophile *Archaeoglobus fulgidus*, *J. Mol. Biol. 320*, 129−142.
53. Pannone, B. K., Kim, S. D., Noe, D. A., and Wolin, S. L. (2001) Multiple functional interactions between components of the Lsm2-Lsm8 complex, U6 snRNA, and the yeast La protein, *Genetics 158*, 187−196.
54. Toro, I., Thore, S., Mayer, C., Basquin, J., Seraphin, B., and Suck, D. (2001) RNA binding in an Sm core domain: X-ray structure and functional analysis of an archaeal Sm protein complex, *EMBO J. 20*, 2293−2303.
55. Mattaj, I. W. (1993) RNA recognition: a family matter? *Cell 73*, 837−840.
56. Schumacher, M. A., Pearson, R. F., Moller, T., Valentin-Hansen, P., and Brennan, R. G. (2002) Structures of the pleiotropic translational regulator Hfq and an Hfq-RNA complex: a bacterial Sm-like protein, *EMBO J. 21*, 3546−3556.

57. Thore, S., Mayer, C., Sauter, C., Weeks, S., and Suck, D. (2003) Crystal structures of the *Pyrococcus abyssi* Sm core and its complex with RNA. Common features of RNA binding in archaea and eukarya, *J. Biol. Chem. 278*, 1239−1247.

58. Valentin-Hansen, P., Eriksen, M., and Udesen, C. (2004) The bacterial Sm-like protein Hfq: a key player in RNA transactions, *Mol. Microbiol. 51*, 1525−1533.

BI048578Z